

# Influence of particle shape models on T-matrix light scattering simulation

Jens Hellmers<sup>a,\*</sup>, Thomas Wriedt<sup>b</sup>

<sup>a</sup>*Universität Bremen, Badgasteiner Str. 3, 28359 Bremen, Germany*

<sup>b</sup>*Institut für Werkstofftechnik, Badgasteiner Str. 3, 28359 Bremen, Germany*

---

## Abstract

Simulation of light scattering gets more and more important; topics of interest are for example characterization of the shape of particles, detection of airborne fibers, determination of spherical and non-spherical particles, etc. To develop advanced methods for optical particle characterization corresponding light scattering theories and simulation programs are needed. For these kinds of simulations adequate input data representing the particle shape is important. If a specific particle shape is obtained from some reconstruction method the model will only be an approximation of the real shape. So the quality of this input particle shape has influence on the quality of the obtained results.

In our research we concentrate on the development of the null-field method with discrete sources for light scattering simulation. With this method the T-matrix of complex structured particles can be computed. This paper gives an overview of solving light scattering problems with the null-field method with discrete sources and shows the influence of the accuracy of the particle shape model on the computed scattering results.

© 2004 Elsevier Ltd. All rights reserved.

*Keywords:* Electromagnetic scattering; T-matrix; Surface discretization

---

## 1. Introduction

In recent years there is much interest in light scattering by real shaped particles. Particles of interest are natural aerosol particles such as Sahara dust or maritime salt crystals, artificial aerosol

---

\*Corresponding author. Tel.: +49-421-2185418; fax: +49-421-2185378.

*E-mail address:* [hellmers@iwt.uni-bremen.de](mailto:hellmers@iwt.uni-bremen.de) (J. Hellmers).

particles such as asbestos or glass fibers, interstellar dust particles, biological cells or technical microparticles and crystals. As it is hardly possible to compute scattering by real shaped particles, investigations are mainly restricted to measurements [1]. But only scattering of ensembles of particles can be investigated in this way. In scattering computations there is up to now a restriction to some rotational symmetric particle shapes such as the sphere, spheroid and finite cylinder although more sophisticated particle shape models such as the ellipsoid [2], cube [3], superellipsoid [4] and gaussian random sphere [5] are becoming available. There are only a few papers demonstrating that the particle shape of a real particle can be reconstructed to do scattering computation. Kocifai [6] reconstructed the shape of an interstellar dust particle from electron microscopy and used the discrete dipole method for scattering computation. Wriedt [7] reconstructed the shape of a pebble and used the *null field method with discrete sources* for scattering computations of a scaled down version of the pebble shape. One major question in scattering computation of real shaped particles is how well the particle shape has to be reconstructed so that scattering computation for such a model approximates the scattering by the exact shape reasonably well. As quite often the reconstruction is based on a triangle surface patch model the question is how many triangular faces are needed to obtain good scattering results. We like to investigate this problem by looking into scattering by a particle approximated by a number of triangular faces. Scattering computations will be based on the *null field method with discrete sources*. The theory will be explained in the first part of the paper. Next, we will look into the problem of scattering by a sphere approximated by a number of triangular faces. The second particle shape we will investigate is an ellipsoid.

## 2. Null field method with discrete sources

The *null field method with discrete sources* is an extension of the well-known T-matrix method. The latter is also called null field method or extended boundary condition method and was developed by Waterman [8]. It is based on an expansion of the incident, transmitted and the scattered field into a series of spherical vector wave functions. For the conventional T-matrix method fast computer codes are easily available [9,10], but they are restricted to scattering by axisymmetric scatterers. For particles with extreme geometries or particles with appreciable concavities the single spherical coordinate based null-field method fails to converge. To cope with this limitations and to improve numerical stability a number of modifications to the conventional null-field method have been developed into the *null field method with discrete sources* [11]. Here a number of elementary sources are used for approximating the surface current densities. The discrete sources are placed on a certain support in an additional region with respect to the region where the solution is required. Unknown discrete sources amplitudes which produce the surface densities are computed by using the null-field condition of the total electric field inside the particle surface. This enables to compute scattering by highly elongated or flat scatterers such as fibers and plates [12] and layered particles [13]. Also the standard T-matrix can be computed [14] for post-processing such as cluster scattering or orientation averaging. The *null field method with discrete sources* has been extended for scattering computation by non-axisymmetric scatterers [15] and the method has been validated by comparison to other methods [16] giving results for cubes.

Given is a three-dimensional space  $D$  with a closed surface  $S$ , its interior  $D_i$  and exterior  $D_s$ .  $k_t = k\sqrt{\varepsilon_t\mu_t}$  is the wave number in the domain  $D_t$ , with  $k = \omega/c$  and  $t = s, i$ . The electric and magnetic fields  $\mathbf{E}_0, \mathbf{H}_0$  shall be an entire solution to the Maxwell equations representing the incident electromagnetic field. Now find the scattered vector fields,  $\mathbf{E}_s, \mathbf{H}_s \in C^1(D_s) \cap C(\overline{D}_s)$  and internal vector fields  $\mathbf{E}_i, \mathbf{H}_i \in C^1(D_i) \cap C(\overline{D}_i)$  satisfying the Maxwell's equations

$$\nabla \times \mathbf{E}_t = jk\mu_t\mathbf{H}_t, \quad \nabla \times \mathbf{H}_t = -jk\varepsilon_t\mathbf{E}_t \tag{1}$$

in  $D_t$  and two boundary conditions

$$\mathbf{n} \times \mathbf{E}_i - \mathbf{n} \times \mathbf{E}_s = \mathbf{n} \times \mathbf{E}_0, \quad \mathbf{n} \times \mathbf{H}_i - \mathbf{n} \times \mathbf{H}_s = \mathbf{n} \times \mathbf{H}_0, \tag{2}$$

on the surface of the scatterer  $S$ . The scattered field  $\mathbf{E}_s, \mathbf{H}_s$  must satisfy the Silver–Müller radiation condition uniformly for all directions  $\mathbf{x}/x$ . The transmission boundary-value problem possesses a unique solution [17]. Now a set of surface current densities  $\mathbf{e}$  and  $\mathbf{h}$  replaces the scattering object, so that in the exterior domain the sources and fields are exactly the same as those existing in the original scattering problem. In the next step a set of integral equations for the surface current densities  $\mathbf{e}$  and  $\mathbf{h}$  is derived for a variety of discrete sources. As discrete sources localized vector spherical functions, distributed vector spherical functions, magnetic and electric dipoles or vector Mie-potentials can be used depending on the specific scattering problem [11]. Physically, this set of integral equations guarantees the null-field condition within  $D_i$ . Essentially, the null-field method with discrete sources consists in the projection relations

$$\int_S \left[ (\mathbf{e} - \mathbf{e}_0) \cdot \Psi_v^3 + j\sqrt{\frac{\mu_s}{\varepsilon_s}}(\mathbf{h} - \mathbf{h}_0) \cdot \Phi_v^3 \right] dS = 0, \\ \int_S \left[ (\mathbf{e} - \mathbf{e}_0) \cdot \Phi_v^3 + j\sqrt{\frac{\mu_s}{\varepsilon_s}}(\mathbf{h} - \mathbf{h}_0) \cdot \Psi_v^3 \right] dS = 0, \quad v = 1, 2, \dots, \tag{3}$$

where  $\mathbf{e}_0 = \mathbf{n} \times \mathbf{E}_0$  and  $\mathbf{h}_0 = \mathbf{n} \times \mathbf{H}_0$  are the tangential components of the incident electric and magnetic fields. The set  $\{\Psi_v^3, \Phi_v^3\}_{v=1,2,\dots}$  consists of radiating solutions to Maxwell equations and depends on the system of discrete sources which is used for imposing the null-field condition. In our case this set together with the set of regular solutions to Maxwell equations  $\{\Psi_v^1, \Phi_v^1\}_{v=1,2,\dots}$  stands for localized vector spherical functions  $\{\mathbf{M}_{mn}^{1,3}, \mathbf{N}_{mn}^{1,3}\}_{m \in \mathbf{Z}, n \geq \max(1, |m|)}$ ,

$$\mathbf{M}_{mn}^{1,3}(k\mathbf{x}) = \sqrt{D_{mn}}z_n(kr) \left[ jm \frac{P_n^{|m|}(\cos \theta)}{\sin \theta} \mathbf{e}_\theta - \frac{dP_n^{|m|}(\cos \theta)}{d\theta} \mathbf{e}_\varphi \right] e^{jm\varphi}, \\ \mathbf{N}_{mn}^{1,3}(k\mathbf{x}) = \sqrt{D_{mn}} \left\{ n(n+1) \frac{z_n(kr)}{kr} P_n^{|m|}(\cos \theta) e^{jm\varphi} \mathbf{e}_r \right. \\ \left. + \frac{[krz_n(kr)]'}{kr} \left[ \frac{dP_n^{|m|}(\cos \theta)}{d\theta} \mathbf{e}_\theta + jm \frac{P_n^{|m|}(\cos \theta)}{\sin \theta} \mathbf{e}_\varphi \right] \right\} e^{jm\varphi}, \tag{4}$$

where  $(\mathbf{e}_r, \mathbf{e}_\theta, \mathbf{e}_\varphi)$  are the unit vectors in spherical coordinates,  $z_n$  designates the spherical Bessel functions  $j_n$  or the spherical Hankel functions of the first kind  $h_n^1$ ,  $P_n^{|m|}$  denotes the associated Legendre polynomial of order  $n$  and  $m$ , and  $D_{mn}$  is a normalization constant given by

$$D_{mn} = \frac{2n+1}{4n(n+1)} \cdot \frac{(n-|m|)!}{(n+|m|)!}. \tag{5}$$

Now the surface current densities are approximated by fields of discrete sources. So let  $\mathbf{e}$  and  $\mathbf{h}$  solve the null-field equations (3) and the system  $\{\mathbf{n} \times \boldsymbol{\Psi}_\mu^1, \mathbf{n} \times \boldsymbol{\Phi}_\mu^1\}_{\mu=1}^\infty$  form a Schauder basis in  $\mathcal{L}_{\tan}^2(\mathcal{S})$ . Then there exists a sequence  $\{a_\mu, b_\mu\}_{\mu=1}^\infty$  such that

$$\begin{aligned}\mathbf{e}(\mathbf{y}) &= \sum_{\mu=1}^{\infty} a_\mu \mathbf{n} \times \boldsymbol{\Psi}_\mu^1(k_i \mathbf{y}) + b_\mu \mathbf{n} \times \boldsymbol{\Phi}_\mu^1(k_i \mathbf{y}), \quad \mathbf{y} \in S, \\ \mathbf{h}(\mathbf{y}) &= -j \sqrt{\frac{\varepsilon_i}{\mu_i}} \sum_{\mu=1}^{\infty} a_\mu \mathbf{n} \times \boldsymbol{\Phi}_\mu^1(k_i \mathbf{y}) + b_\mu \mathbf{n} \times \boldsymbol{\Psi}_\mu^1(k_i \mathbf{y}), \quad \mathbf{y} \in S.\end{aligned}\quad (6)$$

A system  $\{\psi_i\}_{i=1}^\infty$  is called a Schauder basis of a Banach space  $X$  if any element  $u \in X$  can be uniquely represented as  $u = \sum_{i=1}^\infty \alpha_i \psi_i$ , where the convergence of the series is in the norm of  $X$ . In the case of localized vector spherical functions the notion of Schauder basis is closely connected with the Rayleigh hypothesis, which says that the series representation of the scattered field in terms of radiating localized vector spherical functions, which uniformly converges outside the circumscribing sphere, also converges on  $S$ . In the last step the scattered field outside the circumscribing sphere is obtained by using the representation theorem

$$\mathbf{E}_s(\mathbf{x}) = \sum_{v=1}^{\infty} f_v \mathbf{M}_v^3(k_s \mathbf{x}) + g_v \mathbf{N}_v^3(k_s \mathbf{x}), \quad (7)$$

where

$$\begin{aligned}f_v &= \frac{jk_s^2}{\pi} \int_S \left[ \mathbf{e}(\mathbf{y}) \cdot \mathbf{N}_{\bar{v}}^1(k_s \mathbf{y}) + j \sqrt{\frac{\mu_s}{\varepsilon_s}} \mathbf{h}(\mathbf{y}) \cdot \mathbf{M}_{\bar{v}}^1(k_s \mathbf{y}) \right] dS(\mathbf{y}), \\ g_v &= \frac{jk_s^2}{\pi} \int_S \left[ \mathbf{e}(\mathbf{y}) \cdot \mathbf{M}_{\bar{v}}^1(k_s \mathbf{y}) + j \sqrt{\frac{\mu_s}{\varepsilon_s}} \mathbf{h}(\mathbf{y}) \cdot \mathbf{N}_{\bar{v}}^1(k_s \mathbf{y}) \right] dS(\mathbf{y}).\end{aligned}\quad (8)$$

$\bar{v}$  is a complex index incorporating  $-m$  and  $n$ , i.e.  $\bar{v} = (-m, n)$ .

For deriving the T-matrix the incident field shall be expressed inside a finite region containing  $S$  as a series of regular vector spherical functions

$$\begin{aligned}\mathbf{E}_0(\mathbf{x}) &= \sum_{v=1}^{\infty} a_v^0 \mathbf{M}_v^1(k_s \mathbf{x}) + b_v^0 \mathbf{N}_v^1(k_s \mathbf{x}), \\ \mathbf{H}_0(\mathbf{x}) &= -j \sqrt{\frac{\varepsilon_s}{\mu_s}} \sum_{v=1}^{\infty} a_v^0 \mathbf{N}_v^1(k_s \mathbf{x}) + b_v^0 \mathbf{M}_v^1(k_s \mathbf{x}).\end{aligned}\quad (9)$$

Eqs. (3)–(9) show that the relation between the scattered and the incident field coefficients is linear and can be expressed by a transition matrix  $\mathbf{T}$

$$\begin{bmatrix} f_v \\ g_v \end{bmatrix} = \mathbf{T} \begin{bmatrix} a_v^0 \\ b_v^0 \end{bmatrix} \quad (10)$$

with

$$\mathbf{T} = \mathbf{B} \mathbf{A}^{-1}. \quad (11)$$

**A** and **B** are block matrices

$$\mathbf{B} = \begin{bmatrix} \mathbf{B}_{v\mu}^{11} & \mathbf{B}_{v\mu}^{12} \\ \mathbf{B}_{v\mu}^{21} & \mathbf{B}_{v\mu}^{22} \end{bmatrix}, \quad \mathbf{A} = \begin{bmatrix} \mathbf{A}_{v\mu}^{11} & \mathbf{A}_{v\mu}^{12} \\ \mathbf{A}_{v\mu}^{21} & \mathbf{A}_{v\mu}^{22} \end{bmatrix}, \quad v, \mu = 1, 2, \dots \quad (12)$$

Explicit expressions for the block elements of matrices **A** and **B** are given by

$$\begin{aligned} A_{v\mu}^{11} &= \int_S [(\mathbf{n} \times \mathbf{M}_\mu^1) \cdot \mathbf{M}_v^3 + M(\mathbf{n} \times \mathbf{N}_\mu^1) \cdot \mathbf{N}_v^3] dS, \\ A_{v\mu}^{12} &= \int_S [(\mathbf{n} \times \mathbf{N}_\mu^1) \cdot \mathbf{M}_v^3 + M(\mathbf{n} \times \mathbf{M}_\mu^1) \cdot \mathbf{N}_v^3] dS, \\ A_{v\mu}^{21} &= \int_S [(\mathbf{n} \times \mathbf{M}_\mu^1) \cdot \mathbf{N}_v^3 + M(\mathbf{n} \times \mathbf{N}_\mu^1) \cdot \mathbf{M}_v^3] dS, \\ A_{v\mu}^{22} &= \int_S [(\mathbf{n} \times \mathbf{N}_\mu^1) \cdot \mathbf{N}_v^3 + M(\mathbf{n} \times \mathbf{M}_\mu^1) \cdot \mathbf{M}_v^3] dS, \end{aligned} \quad (13)$$

$$\begin{aligned} B_{v\mu}^{11} &= \frac{jk_s^2}{\pi} \int_S [(\mathbf{n} \times \mathbf{M}_\mu^1) \cdot \mathbf{N}_v^3 + M(\mathbf{n} \times \mathbf{N}_\mu^1) \cdot \mathbf{M}_v^3] dS, \\ B_{v\mu}^{12} &= \frac{jk_s^2}{\pi} \int_S [(\mathbf{n} \times \mathbf{N}_\mu^1) \cdot \mathbf{N}_v^3 + M(\mathbf{n} \times \mathbf{M}_\mu^1) \cdot \mathbf{M}_v^3] dS, \\ B_{v\mu}^{21} &= \frac{jk_s^2}{\pi} \int_S [(\mathbf{n} \times \mathbf{M}_\mu^1) \cdot \mathbf{M}_v^3 + M(\mathbf{n} \times \mathbf{N}_\mu^1) \cdot \mathbf{N}_v^3] dS, \\ B_{v\mu}^{22} &= \frac{jk_s^2}{\pi} \int_S [(\mathbf{n} \times \mathbf{N}_\mu^1) \cdot \mathbf{M}_v^3 + M(\mathbf{n} \times \mathbf{M}_\mu^1) \cdot \mathbf{N}_v^3] dS, \end{aligned} \quad (14)$$

with refractive index  $M = \sqrt{\varepsilon_i/\varepsilon_s}$ .

Energy characteristics in the far field can be computed from the far-field pattern  $\mathbf{E}_{s0}^N$  for an unit amplitude incident electric field for p- or s-polarization. The angle-dependent intensity function plotted in the simulation section is the normalized differential scattering cross-section (DSCS)

$$\frac{\sigma_d}{\pi a^2} = \frac{|k_s \mathbf{E}_{s0}^N|^2}{\pi |k_s a|^2}. \quad (15)$$

Three integrals with respect to the three Euler angles  $\alpha, \beta, \gamma$  have to be computed to numerically compute orientation averaged scattering. The value of interest  $f(\alpha, \beta, \gamma)$  is integrated over all directions and polarizations of the incident plane wave. The numerical procedure used for this is based on a step wise procedure

$$\begin{aligned} &\int_0^{2\pi} \int_0^\pi \int_0^{2\pi} f(\alpha, \beta, \gamma) d\alpha \sin \beta d\beta d\gamma \\ &\approx \sum_{n_\alpha=1}^{N_\alpha} \sum_{n_\beta=1}^{N_\beta} \sum_{n_\gamma=1}^{N_\gamma} f(\alpha, \beta, \gamma) \sin(n_\beta \pi / N_\beta) \frac{n_\alpha 2\pi n_\beta \pi n_\gamma 2\pi}{N_\alpha N_\beta N_\gamma}. \end{aligned} \quad (16)$$

The triple integral is converted to three summations. Angle  $\alpha$  is digitized for  $N_\alpha$  steps in the range  $(0, 2\pi)$ , angle  $\beta$  is digitized for  $N_\beta$  steps in the range  $(0, \pi)$ , and angle  $\gamma$  is digitized for  $N_\gamma$  steps in the range  $(0, 2\pi)$ .

### 3. Numerical simulations

#### 3.1. Program validation—sphere

For checking validity of the used programs preliminary simulations for a sphere were done. The achieved results were compared with results for corresponding parameters by Mie—Theory.

Fig. 1 shows an remarkable accordance between the results of the T-matrix simulation of a sphere with 1280 surface patches and Mie theory. So T-matrix method combined with null-field method with discrete sources proofed their applicability for simulating a sphere with a mentionable big dimension. Investigation with more surface patches than 1280 did not produce better results and therefore are not shown here.

#### 3.2. Influence of input particle shape data on simulation results

When simulating light scattering of a given real, arbitrarily particle shape it is necessary to reduce this shape to a construct which is mathematically computable. Especially when trying to convert a real shape to such a model by reconstruction from different views the quality of this reduction is an important issue.

Usually a particle shape is triangulated into a number of triangular surface patches. This kind of triangular surface patches we would like to call from now on triangular faces. The higher the number of used triangular faces the more exact the particle shape will be—see Fig. 2. Here the real

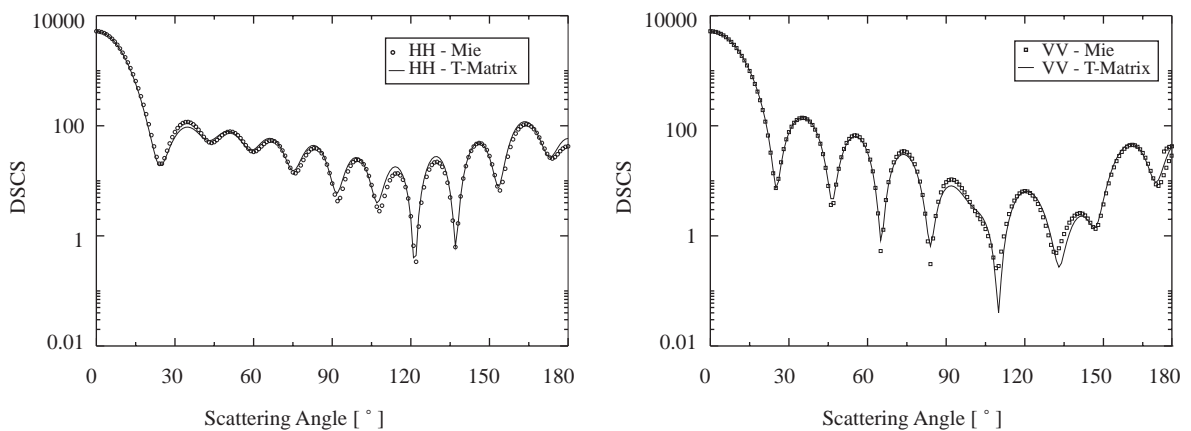


Fig. 1. Differential scattering cross-section for a sphere  $d = 2 \mu\text{m}$ ,  $M = 1.5$ ,  $\lambda = 628.31 \text{ nm}$ . The sphere for T-matrix simulation consists of 1280 triangular surface patches;  $N_{\text{rank}} = 20$ ,  $M_{\text{rank}} = 12$ .  $N_{\text{rank}}$  is the expansion order that determines the dimension of the T-matrix,  $M_{\text{rank}}$  determines the number of azimuthal modes. For better overview the absolute results for T-matrix simulation are scaled so that they fit into the range of Mie results.

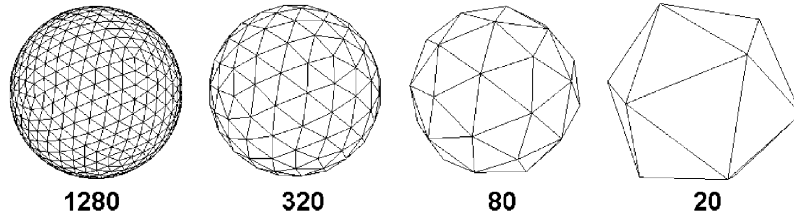


Fig. 2. Sphere approximated by different numbers of triangular faces.

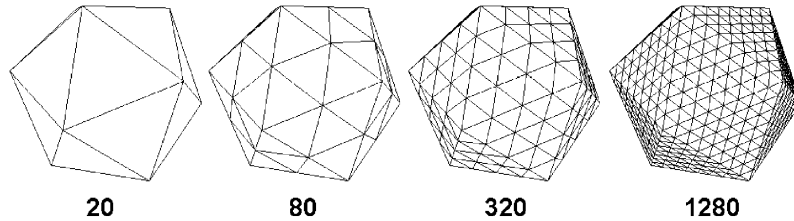


Fig. 3. Sphere with 20 triangular faces—division of faces and addition of triangular patches.

shape is a sphere which is reconstructed with a different number of triangular faces. While 1280 faces produce a good reconstruction the particle shape consisting of 20 triangular faces hardly can be called a sphere.

Unfortunately the quality of the computational results not just depends on the smoothness of the shape. For reasonable, converging T-matrix results a certain amount of triangles is needed to compute surface integrals. To have a sufficient number of triangular patches one can insert additional surface elements mathematically. This of course should not change the shape of the model (Fig. 3). In this case adding of surface elements is done by an algorithm that subdivides the given elements by four. This has the advantage that all the gained elements are of same size and shape. This kind of elements we would like to call triangular patches.

Because a long-term objective of all scattering simulations is the largely accordance with real life, we would like to do some investigations regarded to the mentioned problems. Therefore we take a sphere consisting of 320 triangular faces (Fig. 2) and compare the T-matrix result with the results we got from Mie theory (Fig. 1). The results are presented in Fig. 4. For better clearness only HH polarization is shown. To achieve convergence we had to increase the number of triangular patches by subdividing the triangular faces to get also a total number of 1280 triangular patches. While a sphere consisting of 1280 triangular faces delivers quite good scattering results in comparison with Mie theory as seen in Fig. 1 the same input data reduced to 320 triangular faces leads to results which are mediocre at best (Fig. 4).

Now for a regular sphere—as it is the case with Mie-simulation—it is irrelevant where the incident plane wave hits the surface. But the less smooth the simulated particle appears, the orientation of the particle gets more and more influence. To consider this we calculate the orientation average of scattered light for shapes shown in Fig. 2 and compare this results with Mie results.

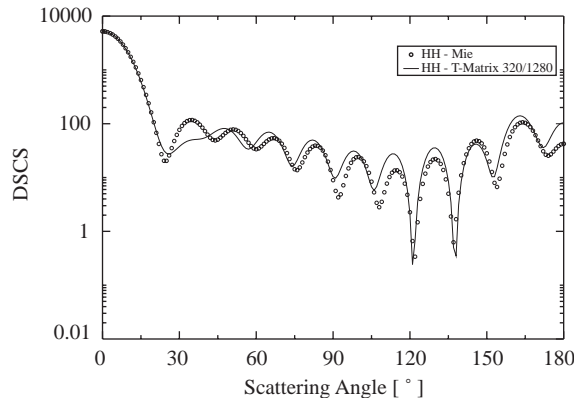


Fig. 4. Comparison between Mie and T-matrix simulation—influence of smoothness and integration areas. Sphere consisting of 320 triangular faces and 1280 triangular patches.  $d = 2 \mu\text{m}$ ,  $M = 1.5$ ,  $\lambda = 628.31 \text{ nm}$ ;  $N_{\text{rank}} = 20$ ,  $M_{\text{rank}} = 12$  in both cases.

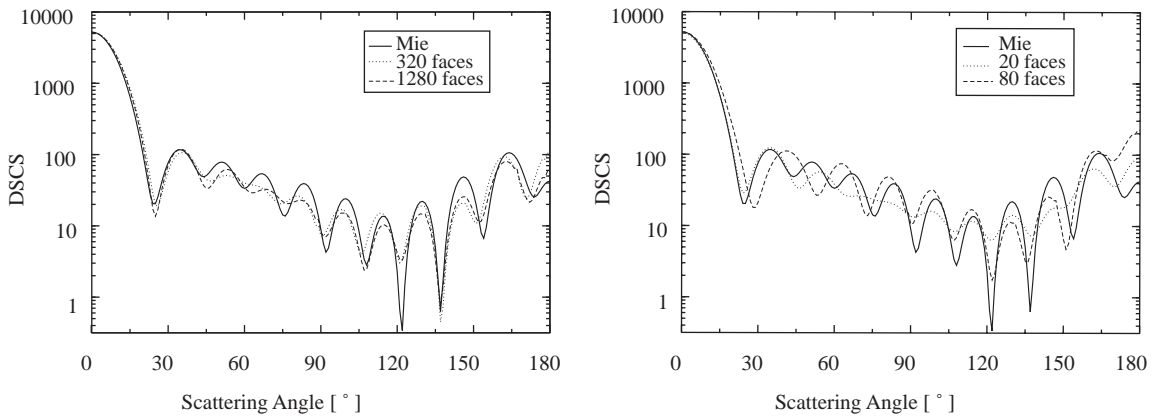


Fig. 5. Comparison between Mie and T-matrix simulation—orientation average of HH polarization for approximated spheres consisting of 1280 triangular patches with different numbers of triangular faces. Left: spheres consisting of 1280 and 320 triangular faces. Right: spheres consisting of 80 and 20 triangular faces.  $d = 2 \mu\text{m}$ ,  $M = 1.5$ ,  $\lambda = 628.31 \text{ nm}$ ;  $N_{\text{rank}} = 20$ ,  $M_{\text{rank}} = 12$  in both cases.  $\theta_{\text{incident}} = 0^\circ$ .

We choose a number 1280 triangular patches—which has shown to be enough for plausible results—to make sure that there is no influence by different numbers of triangular patches.

At first sight it seems that orientation average decreases accuracy of the simulation result for T-matrix simulation of the sphere with 1280 triangular faces and patches (Fig. 5). Compared to this even the sphere consisting of just 80 triangular faces seems to produce better results. To check this impression by a more mathematical estimation we would like to use two different methods. First, we compare the absolute and the relative difference between Mie and T-matrix simulation. Absolute means the difference gained by simple subtraction of T-matrix results from Mie results; relative considers this difference in relation to the Mie result by setting the regarding Mie value as 100%.

Fig. 6 shows that the assumption that a sphere consisting of 80 triangular faces produces as good or even better results as a sphere consisting of 1280 faces was a mistake. The output graph for 1280 faces is the most flat and does not show so high regional difference than any other graph. In general one can see what was expected: the smoother the simulated shape is, the more flat the output graph runs and the less regional peaks are. To put this into an even more mathematical statement we would like to make an assumption by linear regression. Therefore we construct a diagram with the Mie results on  $x$ -axis and the corresponding T-matrix results on  $y$ -axis. Then we do a linear regression which leads to a regression formula

$$y = a + b \cdot x. \tag{17}$$

Here  $a$  stands for the mean value and  $b$  for the standard deviation. If one would insert the Mie results itself in such a kind of diagram and does a linear regression the result would be a perfect straight with offset 0 and gradient 1. The corresponding regression formula would be

$$y = 0 + 1 \cdot x. \tag{18}$$

So by taking T-matrix results as  $y$ -axis values and doing linear regression one gets an impression about the accordance of the results.

The results for linear regression in this case are

Sphere consisting of  $y = a + bx$

$$20 \text{ faces} : y = -1.1725 + 0.96885x$$

$$80 \text{ faces} : y = 21.939 + 1.0299x$$

$$320 \text{ faces} : y = 6.2961 + 1.0273x$$

$$1280 \text{ faces} : y = 0.53739 + 1.0215x \tag{19}$$

The corresponding graphs can be seen in Fig. 7.

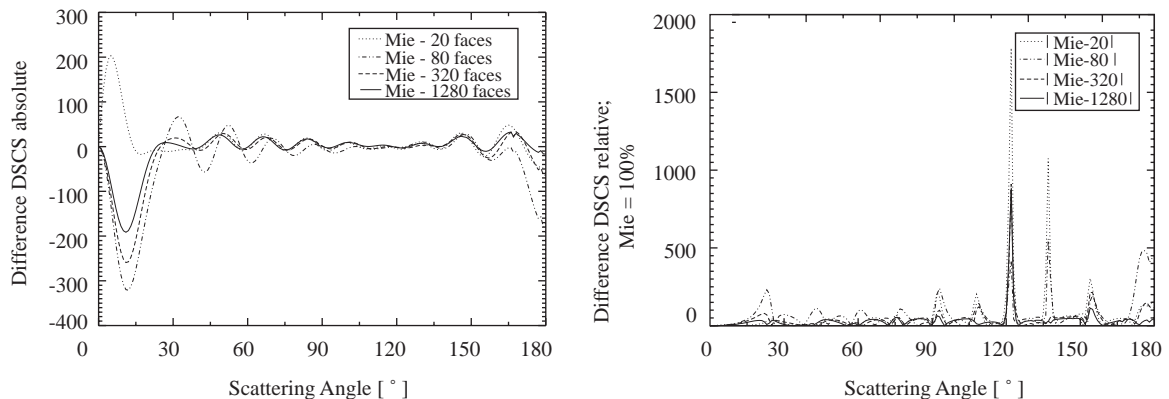


Fig. 6. Difference between Mie and T-matrix simulation—orientation average for approximated spheres consisting of 1280 triangular patches with different numbers of triangular faces. Left: absolute difference by subtraction Mie result—T-matrix result. Right: relative difference by taking the amount of difference of subtraction in relation to Mie result as 100%.  $d = 2 \mu\text{m}$ ,  $M = 1.5$ ,  $\lambda = 628.31 \text{ nm}$ ;  $N_{\text{rank}} = 20$ ,  $M_{\text{rank}} = 12$  in both cases.  $\theta_{\text{incident}} = 0^\circ$ .

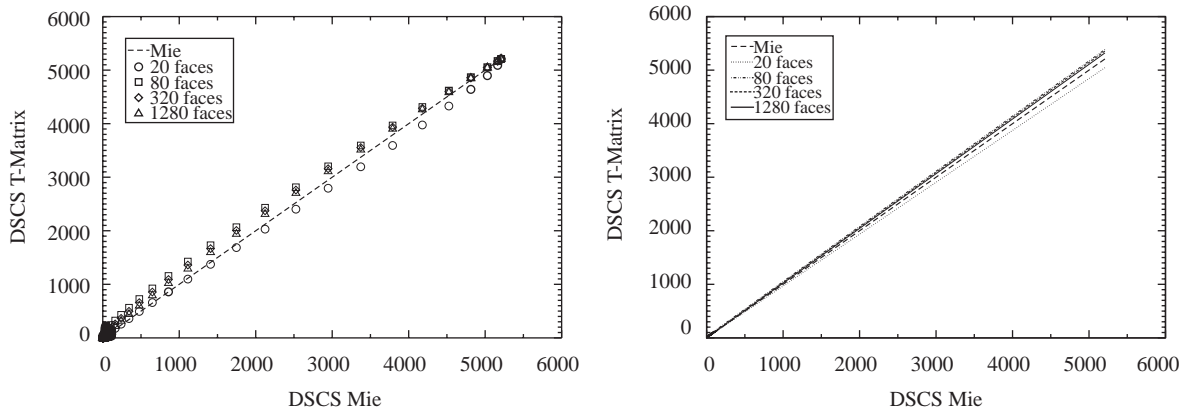


Fig. 7. Difference between Mie and T-matrix simulation—orientation average for approximated spheres consisting of 1280 triangular patches with different numbers of triangular faces. Left: T-matrix results in relation to Mie results. Right: linear regression straights for left diagram.  $d = 2 \mu\text{m}$ ,  $M = 1.5$ ,  $\lambda = 628.31 \text{ nm}$ ;  $N_{\text{rank}} = 20$ ,  $M_{\text{rank}} = 12$  in both cases.  $\theta_{\text{incident}} = 0^\circ$ .

In this way it is possible to estimate the differences by a numerical value. Mean value  $a$  and standard deviation  $b$  are degrees for the accordance. The lower  $a$  the better is the accordance between all simulated T-matrix values compared to Mie; this means for Fig. 6: the more flat the graph becomes. The closer  $b$  to 1 the more homogeneous the T-matrix result is; for Fig. 6: the less peaks can be seen and the graph becomes smoother. Note; to make graphs more easy to survey T-matrix results were scaled so that they fit into the region of Mie results. This means for the standard value  $a$  of T-matrix results that it is not possible to compare them directly and absolute with the 0 that one expects for Mie (18) as  $a$  is influenced by this shift. So it is just a degree to compare T-matrix results to each other. For standard average  $b$  it is a little bit different. Even these values are influenced by the shift, too. So they can be used for a direct comparison with Mie. This is due to the fact how the graph was constructed:  $b$  is a kind of degree for the relation of results between the two simulations. So (19) again confirms the expectations. There is a clear difference between the simulations for different shapes consisting of different numbers of triangular faces. The results get better the more faces the simulated sphere has. One thousand and eighty faces show a good accordance compared with Mie.

### 3.3. Ellipsoid

The null-field method with discrete sources enables to simulate light scattering for a variety of shapes. As another example we would like to present results for an ellipsoid. Again the aim is to investigate the influences mentioned above to find reasonable hints for the quality of shape models to be obtained from reconstruction of real life shapes. For this we simulated light scattering by an ellipsoid with the dimensions of  $x = 800$ ,  $y = 1000$ ,  $z = 1200 \text{ nm}$  (Fig. 8).

Again we changed numbers of triangular faces and patches in different combinations to have a look onto the behavior of corresponding scattering simulation results (Fig. 9).

The T-matrix simulation for 1280 triangular faces produced a very good result compared to Mie theory for a sphere.

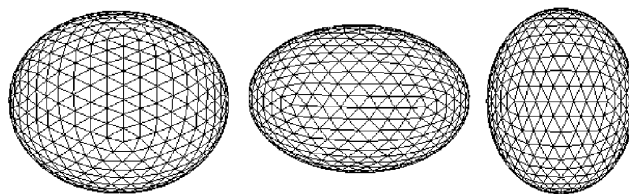


Fig. 8. Simulated ellipsoid; here shown with 1280 surface faces/patches and from 3 different directions. The dimensions are  $x = 800$ ,  $y = 1000$ ,  $z = 1200$  nm.

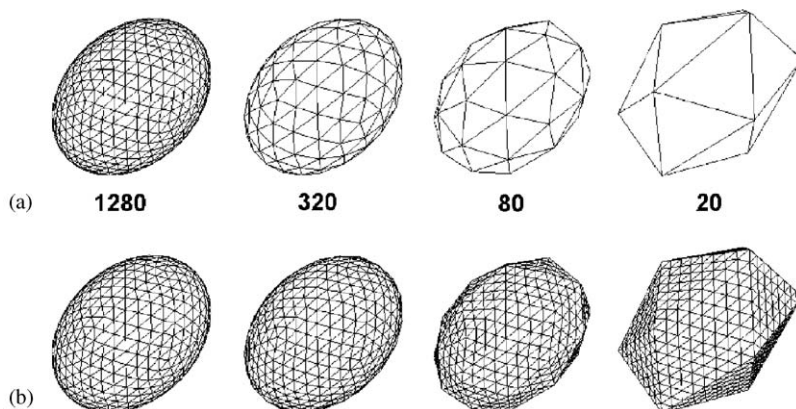


Fig. 9. Simulated ellipsoid—reduction of triangular faces, (a) number of triangular patches is equal to number of triangular faces, (b) number of triangular patches = 1280.

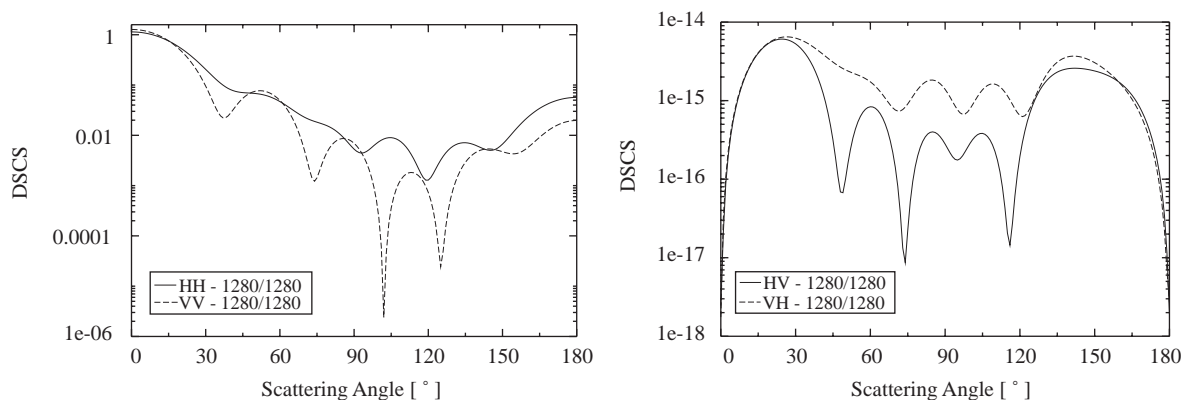


Fig. 10. T-matrix simulation for an ellipsoid consisting of 1280 triangular faces/patches.  $M = 1.5$ ,  $\lambda = 628.31$  nm;  $N_{\text{rank}} = 20$ ,  $M_{\text{rank}} = 12$ .

So in the first step we take an ellipsoid consisting of 1280 surface elements to proof convergence. Fig. 10—left shows the scattering diagram for HH- and VV-polarization. As an ellipsoid has a more complex geometry than a sphere this time we also checked the behavior of

HV- and VH-polarization which is plotted in Fig. 10—right. Convergence was checked both for the number of patches and for the number of expansion functions. It was obtained with 1280 faces as with the sphere on  $N_{\text{rank}} = 20$  and  $M_{\text{rank}} = 12$ . This means that 1280 surface elements again should deliver acceptable results for the approximated ellipsoid. Section 3.2 also showed that the less smooth the simulated shape appears the more influence the direction of incoming light gets. So in the next step we calculate the orientation average for ellipsoids consisting of 1280 triangular patches and 20, 80, 320 and 1280 triangular faces as shown in Fig. 9(b) respectively. These results are plotted in Fig. 11.

Remarkable is the good accordance between the results of 1280 and 320 triangular faces; even the result for 80 triangular faces seems to be good. The result for 20 triangular faces is totally different. This is no wonder—Fig. 9(b) shows that this is a total different shape. But from closer investigation of minima and maxima one can see that the curve shows some similar behavior like the others. When comparing these results with simulation results for a sphere in Fig. 7 one gets the impression that the simulation of an ellipsoid delivers better results. This is due to the fact that the simulated sphere was of bigger dimension. Again we would like to make an assumption by linear regression like in Section 3.2. This time we choose the results for the ellipsoid with 1280 triangular faces as reference. For comparison it is also important again to scale the results. Here they are scaled to the first maximum.

The results for linear regression are

$$\begin{aligned}
 &\text{Ellipsoid consisting of } y = a + bx \\
 &20 \text{ faces : } y = 0.1726 + 0.9644x \\
 &80 \text{ faces : } y = 0.0248 + 1.0170x \\
 &320 \text{ faces : } y = 0.0032 + 1.0046x
 \end{aligned} \tag{20}$$

The corresponding diagrams are shown in Fig. 12.

This confirms again what was expected and could be observed for a sphere. Even without a corresponding simulation result based on Mie theory there is a good chance that the simulation for 1280 triangular faces delivers a reasonable result. The diagrams for 20, 80 and 320 faces show

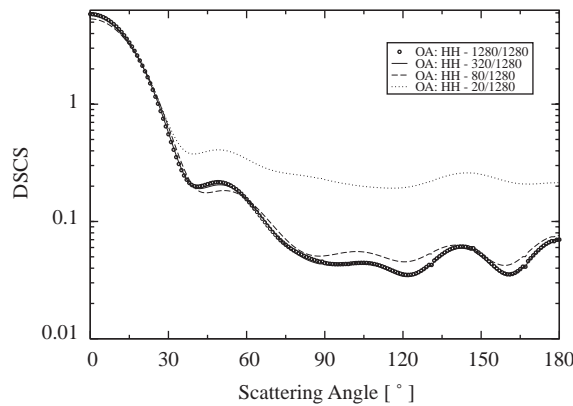


Fig. 11. Comparison of the orientation average for ellipsoids consisting of 1280 triangular patches with different numbers of triangular faces.  $M = 1.5$ ,  $\lambda = 628.31 \text{ nm}$ ;  $N_{\text{rank}} = 20$ ,  $M_{\text{rank}} = 12$  in all cases.  $\theta_{\text{incident}} = 0^\circ$ .

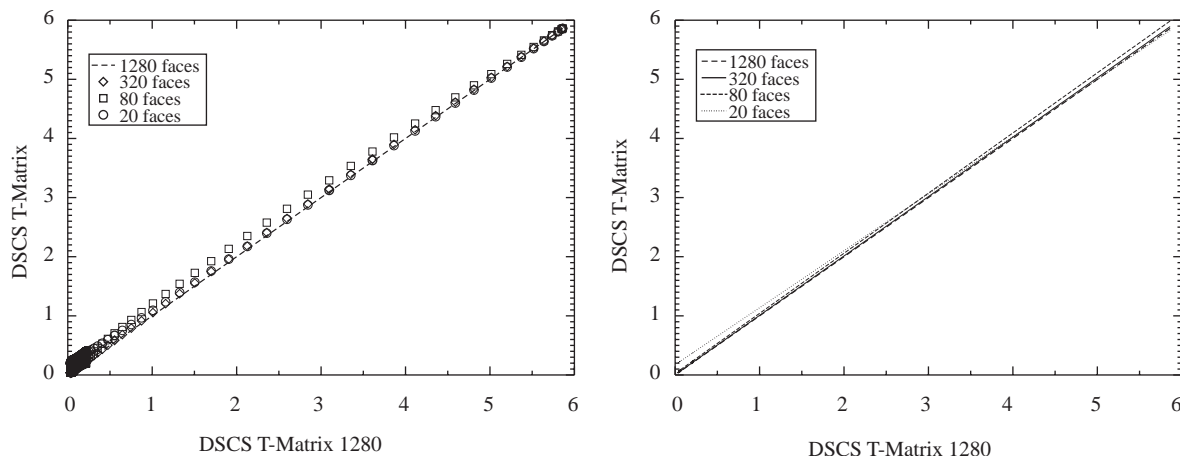


Fig. 12. T-matrix simulation—orientation average for approximated ellipsoids consisting of 1280 triangular patches with different numbers of triangular faces. Left: results in relation to ellipsoid consisting of 1280 patches. Right: linear regression straights for left diagram.  $d = 2 \mu\text{m}$ ,  $M = 1.5$ ,  $\lambda = 628.31 \text{ nm}$ ;  $N_{\text{rank}} = 20$ ,  $M_{\text{rank}} = 12$  in all cases.  $\theta_{\text{incident}} = 0^\circ$ .

the tendency to converge towards the diagram for the simulation of a sphere consisting of 1280 triangular faces, especially the difference in scattering results between 320 and 1280 faces is very small. This is also validated by the regression.

#### 4. Summary and conclusions

In this paper we investigated the influence of input particle shape data on light scattering simulation. We used the *null field method with discrete sources* as an example for a light scattering algorithm which enables to calculate also not so trivial particle shapes like ellipsoids, superellipsoids and cubes. This method is especially appropriate because it relies on the triangular surface elements for surface integral computation. This strong connection between particle shape data and algorithm enables to observe dependences very well. These dependences are especially interesting for cases where a real life shape is reconstructed, e.g. by electron microscopy. But they should also be considered when ‘synthetic’, computer generated shapes are used. For this work we first showed that the *null field method with discrete sources* delivers reasonable results by comparing the light scattering results for a sphere with results attained by Mie theory. It was shown that there is a good accordance for a sphere reconstructed by 1280 triangular faces. So in the next step we reduced the quality of input particle shape data and investigated the changes for light scattering simulation. Of course everybody would expect that the quality of results will decrease if the simulated shape consists of less surface elements. But it gets interesting when looking for Fig. 5. On the first sight it is not so easy to decide how large this loss of quality is. An assumption by linear regression helps to put this differences into numbers and finally shows that a sphere consisting of 320 triangular faces did not produce as bad results as one might expect while spheres with 80 or 20 triangular produced results without any value. The same investigations then were applied on an ellipsoid as input particle shape, leading to the same overall results. So this

means that there is a high chance of getting unwanted results when simulating light scattering because the design of the particle shape one wants to simulate does not correspond to the exact shape. Thereby it is necessary to keep in mind that one can get mathematically correct and converging results—but these might be useless because they belong to a wrong shape. This is an important fact for further work—and not only for scattering simulations done by *null field method with discrete sources*. Especially for cases where light scattering for realistically shaped particles is to be simulated one has to consider the quality of input data—anyway which kind of algorithm or program is used.

## Acknowledgements

We would like to acknowledge support of this work by Deutsche Forschungsgemeinschaft DFG.

## References

- [1] Hovenier JW, Volten H, Munoz O, van der Zande WJ, Waters LBFM. Laboratory studies of scattering matrices for randomly oriented particles. Potentials, problems, and perspectives. *JQSRT* 2003;79-80C:741–55.
- [2] Doicu A, Wriedt T. EBCM with multipole sources located in the complex plane. *Optics Commun* 1997;139:85–98.
- [3] Laitinen H, Lumme K. T-matrix method for general star-shaped particles: first results. *JQSRT* 1998;60:325–34.
- [4] Wriedt T, Doicu A. Light scattering from a particle on or near a surface. *Optics Commun* 1998;152:376–84.
- [5] Muinonen K. Light scattering by axially symmetric Gaussian random particles. In: Videen G, Fu Q, Adelphi PC, editors. Halifax contributions to 5th International Conference on Light Scattering by Nonspherical Particles, August 28 – September 1, 2000. Halifax, Canada: MD; 2000. p. 91–4.
- [6] Kocifai M, Kapisinsky I, Kundracik F. Optical effects of irregular cosmic dust particle U2015 B10. *JQSRT* 1999;63:1–14.
- [7] Wriedt T. Using the T-matrix method for light scattering computations by non-axisymmetric particles: superellipsoids and realistically shaped particles. Part Part Systems Charact 2002;19(4):256–68.
- [8] Waterman PC. Matrix formulation of electromagnetic scattering. *Proc IEEE* 1965;53:805–12.
- [9] Barber PW, Hill SC. Light scattering by particles: computational methods. Singapore: World Scientific; 1990.
- [10] Mishchenko MI, Travis LD. Capabilities and limitations of a current FORTRAN implementation of the T-matrix method for randomly oriented, rotationally symmetric scatterers. *JQSRT* 1998;60:309–24.
- [11] Doicu A, Eremin Y, Wriedt T. Acoustic and electromagnetic scattering analysis using discrete sources. San Diego: Academic Press; 2000.
- [12] Doicu A, Wriedt T. Extended boundary condition method with multipole sources located in the complex plane. *Optics Commun* 1997;139:85–98.
- [13] Doicu A, Wriedt T. Null-field method with discrete sources to electromagnetic scattering from layered scatterers. *Comput Phys Commun* 2001;138:136–42.
- [14] Doicu A, Wriedt T. Calculation of the T-matrix in the null-field method with discrete sources. *J Opt Soc Am A* 1999;16:2539–44.
- [15] Wriedt T, Doicu A. Formulations of the extended boundary condition method for three-dimensional scattering using the method of discrete sources. *J Mod Opt* 1998;45:199–214.
- [16] Wriedt T, Comberg U. Comparison of computational scattering methods. *JQSRT* 1998;60:411–23.
- [17] Müller C. Foundations of the mathematical theory of electromagnetic waves. New York: Springer; 1969.